JOURNAL OF MATERIALS SCIENCE: 33 (1998) 1497–1509

Modelling the three-dimensional elastic constants of parallel-fibred and lamellar bone

U. AKIVA, H. D. WAGNER, S. WEINER*
*Department of Materials and Interfaces, and *Department of Structural Biology, The Weizmann Institute of Science, Rehovot 76100, Israel*
E-mail. cpwagner@wis.weizmann.ac.il

The complex hierarchical structure of lamellar bone makes understanding structure–mechanical function relations, very difficult. We approach the problem by first using the relatively simple structure of parallel-fibred bone to construct a mathematical model for calculating Young's moduli in three-dimensions. Parallel-fibred bone is composed essentially of arrays of mineralized collagen fibrils, which are also the basic structural motif of the individual lamellae of lamellar bone. Parallel-fibred bone structure has orthotropic symmetry. As the sizes and shapes of crystals in bone are not well known, the model is also used to compare the cases of platelet-, ribbon- and sheet-reinforced composites. The far more complicated rotated plywood structure of lamellar bone results in the loss of the orthotropic symmetry of individual lamellae. The mathematical model used circumvents this problem by sub-dividing the lamellar unit into a thin lamella, thick lamella, transition zone between them, and the recently observed ''back-flip'' lamella. Each of these is regarded as having orthotropic symmetry. After the calculation of their Young's moduli they are rotated in space in accordance with the rotated plywood model, and then the segments are combined to present the overall modulus values in three-dimensions. The calculated trends compare well with the trends in microhardness values measured for circumferential lamellar bone. Microhardness values are, as yet, the only measurements available for direct comparison. Although the model is not directly applicable to osteonal bone, which is composed of many hollow cylinders of lamellar bone, the range of calculated modulus values and the trends observed for off-axis calculations, compare well with measured values.

1. Introduction

Relating the mechanical properties of bone to its structure is a very challenging task. Bone occurs in several different forms or types and has a complex hierarchical structure [1, 2]. Furthermore, bone structure, and, in particular, mineral content, changes with increasing age of the bone, and this too has a direct effect on mechanical properties [1, 3, 4]. Bone structure–mechanical relations have, therefore, to be resolved for well-defined bone types of a specific age. Here we address this question first for the relatively simple parallel-fibred bone, and then use this as a basis for addressing the far more complex structure, rotated plywood, that is present in lamellar bone [5]. We approach this by using our current knowledge of the structure as a basis for constructing a mathematical model of the material properties of the bone type, and then compare the calculated results with the few appropriate data sets of experimentally measured values.

This approach has been used in several other studied. Recent examples are the studies of Sasaki *et al.* [6], Wagner and Weiner [7] and Currey *et al.* [8]. Sasaki *et al.* [6] used fibrolamellar bone which is composed of both lamellar and parallel-fibred bone. They measured the preferred orientations of the *c*-axes of the crystals and introduced this information into their model. They, like many earlier studies, assumed that the crystals are needle-shaped. Direct observations [9–13] as well as the modelling studies of Wagner and Weiner [7] and Currey *et al.* [8], both show that most, if not all, the crystals are plate-shaped and that bone should be regarded as a platelet-reinforced composite material. The structure of the narwhal tusk studied by Currey *et al.* [8] is very poorly known, and this limits the extent to which its structure can be related to measured mechanical properties.

Parallel-fibred bone is essentially an array of parallel mineralized collagen fibrils [14]. The plate-shaped crystals within each fibril are arranged in layers that traverse the collagen fibril [15]. The structure of lamellar bone has been the subject of many studies, and was reviewed by Weiner and Traub [2]. Its basic plywood motif has been well documented [16–19] and a well substantiated structural model for collagen fibril organization was proposed by Giraud-Guille [17]. In this model each lamella is composed of arrays of parallel fibrils. The orientations of the fibril arrays in adjacent lamellae are different, thus forming

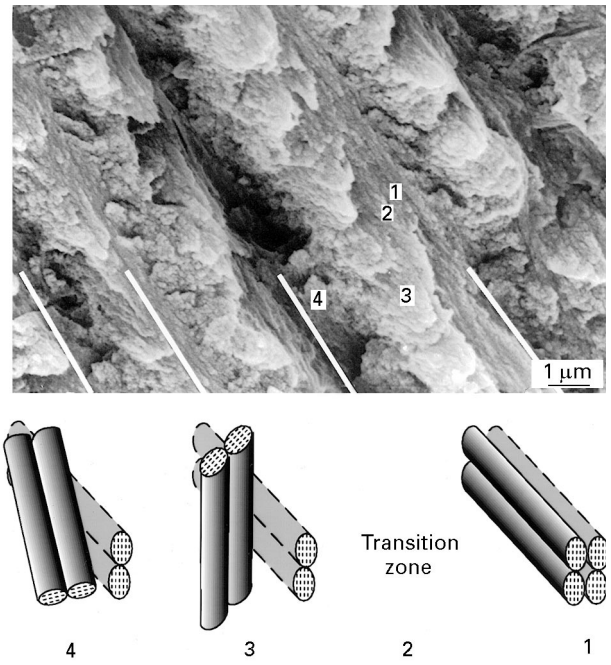

Figure 1 Scanning electron micrograph of the fracture surface of rat tibia lamellar bone (published previous [22]) showing the lamellar units (between white bars), each of which is composed of a thin lamella (1), a transition zone (2), a thick lamella (3) and a "back-flip" lamella" (4). We deliberately use a micrograph published previously [22], to show that the "back-flip" lamella is present, but we did not, at the time, note its significance. For more information, see [53].

a plywood-like motif [16–19]. Note that not all investigators concur with this view of the lamellar structure [20]. Weiner *et al.* [5] observed that the crystal layers are parallel to the lamellar boundary plane in the thin lamellae, but are rotated relative to the lamellar boundary plane in the thick lamella. They therefore called this structure "rotated plywood". This constituted the basis for a model that attempted to relate structure to material properties by Wagner and Weiner [7]. Our understanding of the rotated plywood structure has subsequently been further refined to include more information on the structure of the transition zone between the thick and thin lamellae, the presence of a so-called "back-flip" lamella and semi-quantitative measurements of the plywood angle [21, 22]. The basic features of the structure are shown in Fig. 1.

The models proposed by Sasaki *et al.* [6], Wagner and Weiner [7], Currey *et al.* [8] and indeed the one proposed here, all predict the variations in elastic modulus with changing orientations of the specimen tested in relation to the long axis of the bone. This is a fairly stringent test. A serious problem, however, is the paucity of appropriate experimental measurements of this type. Reilly and Burstein [23], Bonfield and Grynpas [24] and recently Turner *et al.* [25] collected such data for a variety of lamellar bones and fibrolamellar bone. The lamellar bones used were osteonal, which complicates the geometry enormously due to the cylindrical nature of the osteon and its central blood vessel. Fibrolamellar bone is a mixture of two bone types [16], making its interpretations equivocal. Ziv *et al.* [15] performed a detailed microhardness study on circumferential lamellar bone (which is essentially composed of parallel lamellar units) probed in many different orientations with respect to the rotated plywood structure. Microhardness is a convenient tool for doing this, but unfortunately it is difficult to relate hardness values to most other material properties of bone. The trends, however, should be the same. Evans *et al.* [26] made an empirical study of microhardness–Young's modulus relations using many different bones. Although a correlation is observed, we hesitate to use this to convert microhardness values to elastic moduli because the samples were not oriented relative to their structures and many different structures are all lumped together.

Here we present a more refined micromechanical model for the three-dimensional Young's modulus of lamellar bone. The present model follows, at first, the logic of our previous model [7], that is, the focus rests first on the single lamella (parallel-fibred bone in essence), then on bone viewed as an assembly of lamellae. However, regarding the latter, the approach taken here is now fully three-dimensional and eliminates the need for the arbitrary factor, ξ, used in our previous model [7] to account for the weakening effect induced by the rotation of the crystal layers in the thick lamellae.

1.1. Bone structure: comments on the key features incorporated into the model

The basic building block of bone is a mineralized collagen fibril [27], which is composed of thin, plate-shaped crystals of carbonated apatite (dahllite) arranged in parallel layers within the type I collagen fibril [9]. The crystal thicknesses, as measured by small-angle X-ray scattering are about 1.5–3.0 nm [12, 29]. The crystals themselves, once extracted, are very irregular in shape, but are on average 50 nm long by 25 nm wide [11, 13]. Very little, however, is known about their *in vivo* dimensions. As extraction almost certainly causes breakage, they may be much larger, as has been suggested by Boyde [30] who studied ion-beam thinned dentine. We also know very little about the nature of crystal–crystal contacts *in vivo*, and about crystals that may be located between collagen fibrils. The structure of the type I collagen fibril, to a large extent, dictates the organization of the crystals inside the fibril [31]. Although crystals initially form in the gap zones [31–33], they rapidly fill the gap zones, and then spread into the overlap zones [34] ultimately to form extended layers. Following the model for the type I collagen fibril based on stoichiometric measurements of cross-links [35, 36], the layers of crystals are separated by four layers of close-packed triple helical molecules. The distance separating crystal layers is about 4–5 nm [2], based on a fairly prominent 4 nm reflection present in X-ray diffraction patterns of type I collagen [37] and from direct measurements [38]. Note too that the proportions of collagen, crystals and water vary in normal bone from species to species, with the age of the animal, and within the bone as a function of remodelling. This has an important effect on almost all material properties [3, 4]. The relative proportions of collagen,

crystals and water more or less follow a regular pattern [39].

Bundles of parallel mineralized collagen fibrils can be arranged in a variety of ways to form different bone types and associated tissues such as cementum, dentine and mineralized tendon. In this study we focus on two such bone types: the parallel-fibred bone and lamellar bone. In terms of the model, we regard parallel-fibred bone as being composed of an array of mineralized collagen fibrils, aligned not only along their fibril axes, but also in terms of their crystal layers. This highly ordered three-dimensional structure is clearly idealized, and *in vivo* there is almost certainly less order particularly in the azimuthal orientations of the crystal layers [15]. We also use an idealized rotated plywood structure for modelling lamellar bone.

An analysis of the basic features of the rotated plywood structure showed that much of the variation within the structure can be described in terms of two angles, the plywood angle, ψ_1, and the rotation angle, ψ_2 [7]. This relatively simple situation arises because most of the mineralized collagen fibrils are in planes parallel to the boundaries between lamellae. The plywood angle, ψ_1, describes the extent of offset of the collagen fibril axes from one layer of collagen fibrils to the next. The rotation angle, ψ_2, is the extent of rotation about the fibril axis from one layer to the next. Wagner and Weiner [7] arbitrarily defined $\psi_1 = 0$ when the fibrils are perpendicular to long axes of the bone, and $\psi_2 = 0$ when the crystal layers are parallel to the lamellar boundary plane. Weiner *et al.* [21] have measured ψ_1 angles between associated layers using decalcified and vitrified thin sections of the rat femur lamellar bone cut approximately parallel to the lamellar boundary plane. They proposed a model in which the ψ_1 values of a lamellar unit increase in discrete steps of roughly 30°, such that the thick lamella fibrils are roughly orthogonal to those of the thin lamella; a result consistent with other observations [16, 17]. There also appears to be an additional lamella in which the ψ_1 angle is 120°. This "back-flip" lamella borders on the lamellar boundary. In order to simplify this situation, we propose to use the term "lamellar unit" to include the traditional thin and thick lamellae, as well as the transition zone between them and the 120° "back-flip" lamella. The structure of an individual lamellar unit can be seen in Fig. 1. Most of the features described above are incorporated into the theoretical model. The specific values used are, for the most part, for the midshaft of a rat tibia or femur and are listed in Table I.

TABLE I Structural and material parameters of lamellar bone used for the calculations (refer to Figs 1 and 2 for notations)

Structural parameters		Reference
Average crystal platelet dimensions	$50 \times 25 \times 2$ nm^3	[1, 3]
Distance between crystal layers: corresponds to 4 nm spacing in structure ($d = 2$ nm and $2 \times 1/2$ crystal thickness of 2 nm)	$d = 2$ nm	[2, 37]
Lateral space between crystals (assumed to be very small)	$u = 0.1$ nm (parallel to collagen fibril axis)	–
	$v = 0.1$ nm (perpendicular to collagen fibril axis)	–
Calculated (Equation 3) platelet volume fraction (corresponds to 67% ash weight)	$V_p = 0.5$	[15, 39]
Average lamellar unit thickness (rat)	3.2 μm	[21]
Average thick lamella thickness (rat)	1.8 μm	[21]
Average thin lamella thicknes	0.4 μm[a]	[21]
Average transition zone (between thin and thick lamellae) thickness (rat)	0.4 μm[a]	[21]
Average thickness of the "back-flip" lamellae	0.6 μm	[21]
ψ_1 and ψ_2 angles		
Thin lamella	$\psi_1 = 0$ $\psi_2 = 0$	[5]
Transition zone	calculated	–
Thick lamella	$\psi_1 = 90°$ $\psi_2 = 70$[b]	[21]
Back-flip lamella	$\psi_1 = 120°$ $\psi_2 = 90°$	[21]
Material stiffness constants		
Young's modulus of mineral	$E_p = 114$ GPa	[40]
Shear modulus of mineral	$G_p = 44.5$ GPa	[40]
Poisson ratio of mineral (calculated for isotropic platelets)	$\nu_p = 0.30$	–
Young's modulus of collagen	$E_m = 1.5$ GPa	[4]
Shear modulus of collagen	$G_m = 1$ GPa	[41]
Collagen's Poisson's ratio (corresponds to $\nu_{12} = 0.35$ for the overall Poisson's ratio of the collagen–mineral composite calculated using the rule of mixtures)	$\nu_m = 0.38$	[39]

[a] These two zones cannot be differentiated in scanning electron micrographs, so we arbitrarily divided them into two equal halves.
[b] No data are available for ψ_2. Based only on impressions from scanning electron micrographs.

2. Theoretical model

2.1. Elastic constants of parallel-fibred bone

Parallel-fibred bone and an individual lamella of lamellar bone are here regarded as having the same structures.

2.1.1. Platelet and ribbon reinforcement

The structure of the collagen–crystal composite shows that it should be modelled as a unidirectional plane-parallel (UPP) platelet-reinforced composite, rather than a fibre composite. UPP platelet ribbon- or sheet-reinforced composites (where a ribbon has one of its dimensions much larger than a platelet and a sheet has both dimensions much larger than a platelet) have three orthogonal planes of symmetry and, thus, their elastic behaviour is characteristic of three-dimensional orthotropic materials, which possess nine independent elastic constants [42, 43].

Very little theoretical or experimental work has been performed on the elastic properties of platelet- or ribbon-reinforced composites, apart from some results proposed by Halpin [44], a theoretical model by Padawer and Beecher [45], and a model by Lusis *et al.* [46]. Related work by Nielsen [47, 48] is also available. Some elastic constants (like Young's moduli) have been studied more than others, and therefore theoretical models for some constants may not be available. In the following it is assumed that the "1" direction is parallel to the long dimension of the platelet or the ribbon, the "2" direction is perpendicular to the former, within the plane of the platelet or ribbon, and the "3" direction is the out-of-plane direction. The "1" direction *in vivo* is also parallel to the axis of the collagen fibril [10]. We now review the models available for each of the nine elastic constants for the UPP platelet- and ribbon-reinforced composites.

2.1.1.1. Longitudinal Young's modulus, E_1. According to the Halpin–Tsai model [44], the longitudinal (parallel to the long axis of the platelet or ribbon) modulus of a UPP composite is given by

$$E_1 = E_m \frac{1 + ABV_p}{1 - BV_p} \tag{1}$$

where

$$B = \frac{E_p/E_m - 1}{E_p/E_m + A} \tag{2}$$

and where E_m is the matrix modulus, E_p is the platelet (or ribbon) modulus, V_p is the volume fraction of platelet reinforcement, given by

$$V_p = \left(\frac{L}{L+u}\right)\left(\frac{W}{W+v}\right)\left(\frac{T}{T+d}\right) = \left(1+\frac{u}{L}\right)\left(1+\frac{v}{W}\right)\left(1+\frac{d}{T}\right)^{-1} \tag{3}$$

where L is the platelet length, W is the platelet width and T is its thickness, and u, v and d are the longitudinal, transverse in-plane and transverse out-of-plane distances between platelets, respectively (Fig. 2). In particular, for ribbon-reinforced composites ($u \to 0$ and $L \to \infty$)

$$V_p = \left(1+\frac{v}{W}\right)\left(1+\frac{d}{T}\right)^{-1}$$

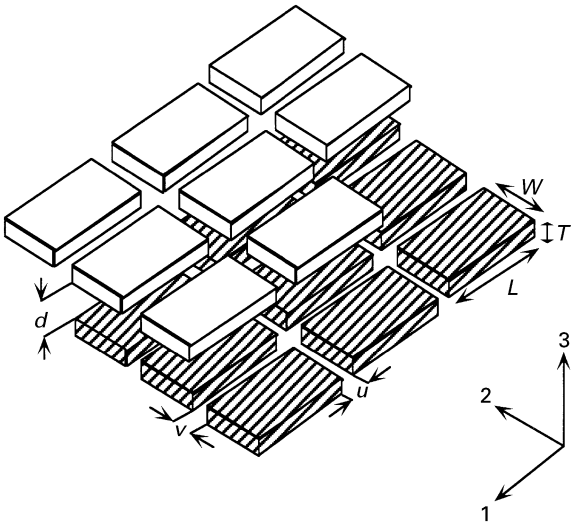

Figure 2 Schematic illustrations of the arrangements of highly stylized platelet-shaped crystals in parallel-fibred bone introducing the geometrical parameters and the defined (1, 2, 3) set of principal axes constituting the model for this specific bone type.

The parameter A in Equations 1 and 2 is given by

$$A = 2\left(\frac{L}{T}\right) + 40V_p^{10} \tag{4}$$

For typical platelet dimensions and platelets volume fraction in bone (Table I) $40V_p^{10} \ll 2(L/T)$. Thus, for a UPP platelet-reinforced "boney" composite $A \approx 2(L/T)$. In the case of ribbon-reinforced composites, $L \to \infty$, thus $A \to \infty$ and (from Equation 2) $B \to 0$ whereas $AB \to (E_p/E_m) - 1$. Equation 1, therefore, transforms into the rule of mixtures

$$E_1 = E_m(1 - V_p) + E_pV_p \tag{5}$$

Other models for Young's modulus, E_1, of platelet-reinforced composites were proposed by Padawer and Beecher [45] and by Lusis *et al.* [46]. Both have similar expressions as follows

$$E_1 = E_m(1 - V_p) + \mu E_pV_p \tag{6}$$

in which, for the Padawer and Beecher (PB) model, $\mu = 1 - [\tanh(n)/n]$, whereas for the Lusis *et al.* (LWX) model, $\mu = 1 - [\ln(n+1)/n]$. In both cases

$$n = \frac{L}{T}\left(\frac{G_m}{E_p}\right)^{1/2}\left(\frac{V_p}{1-V_p}\right)^{1/2} \tag{7}$$

where G_m is the matrix shear modulus, and the other parameters were previously defined. Here also, as for the Halpin and Tsai (HT) scheme (Equation 1), the rule of mixtures is obtained for ribbon-reinforced composites, because $L \to \infty$, $n \to \infty$ and $\mu \to 1$ in both cases. The LWX scheme is essentially a modified version of the PB model, as it takes into account

platelet–platelet interactions at high platelet content. The PB and LWX schemes are based on Cox's early model [9] but they take into account the platelet-like geometry of the reinforcement. Available experimental data (for glass, aluminium diboride and silicon carbide platelets in PB [45] and for phlogopite and muscovite mica flakes in LWX [46] fall short of all schemes due to variability in the geometrical and the structural parameters, but the general trends are quite satisfactory. Thus, three different expressions are available for the calculation of E_1.

2.1.1.2. Transverse in-plane Young's modulus E_2. Three different expressions are also available for the transverse in-plane Young's modulus, E_2, based on the HT, PB, and LWX schemes. The expressions are the same as Equations 1 and 5, but the aspect ratio L/T is now replaced by W/T in Equations 4 and 7. Regarding Equation 4, one has again the simplification $40V_p^{10} \ll 2(W/T)$.

2.1.1.3. Transverse out-of-plane Young's modulus, E_3. The HT model does not offer an expression for the transverse out-of-plane Young's modulus, E_3. PB, LWX models are not relevant here because they deal with the modulus reduction factor, μ, in the plane of reinforcement only. We thus suggest the following approximation for E_3. By interchanging axes 2 and 3, and 1 and 3, one obtains aspect ratios (T/W) and (T/L), respectively. As the length and width of an individual platelet are of the same order of magnitude, and are both much larger than its thickness (Table I), the aspect ratio for E_3, to be used in Equations 4 and 7, is assumed to be $A \approx 2T/(W + L)$. As T gets smaller with respect to W and L, the value of A approaches zero, as indeed was suggested by Nielsen [48] for ribbons. For $A = 0$, Equation 1 becomes the inverse rule of mixtures

$$\frac{1}{E_3} = \frac{V_p}{E_p} + \frac{1 - V_p}{E_m} \tag{8}$$

2.1.1.4. Shear moduli and Poisson's ratios. For the shear moduli, G_{ij}, and the Poisson's ratios ν_{ij} $(i, j = 1, 2, 3 \text{ and } i \neq j)$ the HT equations may be used. Table II lists the values of A used in the HT equations, for the shear moduli and the Poisson's ratios in the cases of platelet or ribbon reinforcement, as suggested by Halpin [44] and Nielsen [48]. Note from Table II that no expressions for A exist for G_{31} and ν_{31} in the case of platelets, and for ν_{12}, ν_{31} in the case of ribbons. For these missing values the following approaches will be taken. Because for ribbon reinforcement $A_{G_{31}} = A_{G_{23}}$ (Table II), we will assume that the same identity is valid for platelet reinforcement. Moreover, because we have $A_{\nu_{12}} = \infty$ for platelet reinforcement, the same will be assumed for ribbon reinforcement. Finally, for both platelet and ribbon reinforcements we will arbitrarily assume that $A_{\nu_{31}} = A_{\nu_{23}} = 0$.

2.1.2. Sheet reinforcement

Sheet reinforcement is the limiting case of very wide ribbons (large aspect ratio W/T), as discussed by Nielsen [47, 48]. Elastic constants for this case, as suggested by Nielsen are

$$E_1 = E_2 = E_p V_p + E_m(1 - V_p); \frac{1}{E_3} = \frac{V_p}{E_p} + \frac{1 - V_p}{E_m} \tag{9}$$

$$G_{12} = G_p V_p + G_m(1 - V_p); \frac{1}{G_{23}} = \frac{1}{G_{31}} = \frac{V_p}{G_p} + \frac{1 - V_p}{G_m} \tag{10}$$

$$\nu_{12} = \nu_p V_p + \nu_m(1 - V_p); \frac{1}{\nu_{23}} = \frac{1}{\nu_{31}} = \frac{V_p}{\nu_p} + \frac{1 - V_p}{\nu_m} \tag{11}$$

where the volume fraction, V_p, now becomes, as $u \to 0$, $v \to 0$ and $L \to \infty$, $W \to \infty$

$$V_p = \left(1 + \frac{d}{T}\right)^{-1} \tag{12}$$

TABLE II Literature values of the parameter A in Equations 1 and 2 for the principal elastic constants of platelet [44] and ribbon [47, 48] reinforced composites

Elastic constant	A (platelets)	A (ribbons)
G_{12}	$\left(\frac{L+W}{2T}\right)^{1.73}$	$\left(\frac{W}{T}\right)^{1.73}$
G_{23}	$\frac{1}{4 - 3\nu_m}$	0
G_{31}	–	0
ν_{12}	∞	–
ν_{23}	0	0
ν_{31}	–	–

2.2. Elastic constants of lamellar bone

The calculation of Young's modulus of lamellar bone must take into account the fact that its basic repeating structure, the lamellar unit, is composed of stacked sets of ordered lamellae comprising a thin lamella, a transition zone, a thick lamella and a fourth 120° "back-flip" lamella. Furthermore, each lamella has a different orientation in space as defined by Ψ_1 and Ψ_2 angles [7]. The relative orientation in space, and thickness, of each lamella are important for accurate numerical estimations of the overall Young's modulus of lamellar bone, using the following approach. We assume [5, 7] that the principal axes of the thin lamella are aligned with the principal axes of bone (Fig. 3) and, thus, the stiffness constants of the thin lamella in the major axes of bone (i.e. bone axis, tangential axis, and radial axis) are merely those of an individual lamella in its principal axes. We will first transform the principal elastic moduli of each of the remaining lamellae in a lamellar unit into their corresponding values along the major axes of bone, then use a rule of mixtures approach to calculate the overall values of the moduli of bone along its principal axes. For the purpose of transforming the elastic moduli of the thick lamella and the "back-flip" lamella

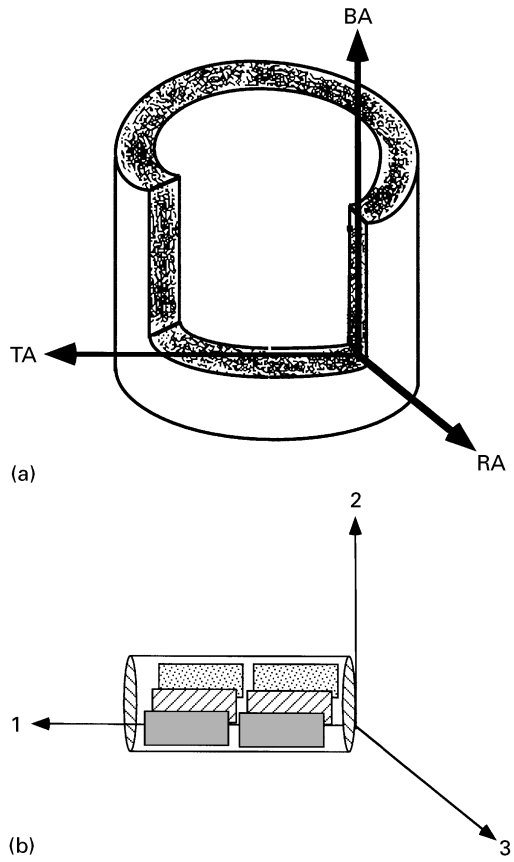

Figure 3 Schematic illustration (top) of the principal axes of a long bone. BA, bone axis; TA, tangential axis; RA, radial axis. The lower schematic illustration shows the orientations of the crystals and the collagen fibrils in the thin lamella in relation to the 3 principal axes.

each along its principal axes (i.e. 1, 2 and 3 axes of individual lamellae as defined above) into their elastic moduli along the major axes of bone, we suggest the following method.

We consider a rectangular system of coordinates (x, y, z) with axes oriented arbitrarily with respect to the principal directions of elasticity (1, 2, 3) of an orthotropic body. Following Lekhnitskii [42], we have a general expression for Young's moduli E_{kk}, shear moduli G_{kl} and Poisson's ratio ν_{kl} with $k, l = x, y, z$ along the arbitrary system of coordinates (x, y, z), in terms of the cosine directors $\alpha_i, \beta_i, \gamma_i$ $(i = 1, 2, 3)$, the corresponding Young's moduli, E_{ii}, and the other elastic constants in the principal axes, ν_{ij}, (Poisson's ratios), and G_{ij} (the shear moduli), as follows ($k, l = x, y, z$, $i, j = 1, 2, 3$ and k and l are linked to i and j, respectively, such that k (or l) $= x$ implies i (or j) $= 1$, k (or l) $= y$ implies i (or j) $= 2$, k (or l) $= z$ implies i (or j) $= 3$)

$$E_{kk} = \left(\frac{\alpha_i^4}{E_1} + \frac{\beta_i^4}{E_2} + \frac{\gamma_i^4}{E_3} + \alpha_i^2\beta_i^2 I_{12} + \beta_i^2\gamma_i^2 I_{23} + \gamma_i^2\alpha_i^2 I_{31}\right)^{-1} \tag{13}$$

where

$$I_{mn} = \frac{1}{G_{mn}} - 2\,\frac{\nu_{mn}}{E_{mm}} \quad (m, n = 1, 2, 3\ m \neq n) \tag{14}$$

$$\frac{1}{G_{kl}} = 4\left(\frac{\alpha_i^2\alpha_j^2}{E_1} + \frac{\beta_i^2\beta_j^2}{E_2} + \frac{\gamma_i^2\gamma_j^2}{E_3}\right) - 8\left(\frac{\nu_{12}}{E_1}\,\alpha_i\alpha_j\beta_i\beta_j + \frac{\nu_{23}}{E_2}\,\beta_i\beta_j\gamma_i\gamma_j + \frac{\nu_{31}}{E_3}\,\gamma_i\gamma_j\alpha_i\alpha_j\right) + \frac{(\alpha_i\beta_j + \alpha_j\beta_i)^2}{G_{12}} + \frac{(\beta_i\gamma_j + \beta_j\gamma_i)^2}{G_{23}} + \frac{(\gamma_i\alpha_j + \gamma_j\alpha_i)^2}{G_{31}} \quad (k \neq l) \tag{15}$$

$$\frac{\nu_{kl}}{E_{ii}} = \left[\frac{\nu_{12}}{E_1}(\alpha_i^2\beta_j^2 + \alpha_j^2\beta_i^2) + \frac{\nu_{23}}{E_2}(\beta_i^2\gamma_j^2 + \beta_j^2\gamma_i^2) + \frac{\nu_{31}}{E_3}(\gamma_i^2\alpha_j^2 + \gamma_j^2\alpha_i^2)\right] - \left(\frac{\alpha_i^2\alpha_j^2}{E_1} + \frac{\beta_i^2\beta_j^2}{E_2} + \frac{\gamma_i^2\gamma_j^2}{E_3} + \frac{\alpha_i\alpha_j\beta_i\beta_j}{G_{12}} + \frac{\beta_i\beta_j\gamma_i\gamma_j}{G_{23}} + \frac{\gamma_i\gamma_j\alpha_i\alpha_j}{G_{31}}\right) \quad (k \neq l) \tag{16}$$

The cosine directors $\alpha_i, \beta_i, \gamma_i$, $i = 1, 2, 3$ determine the position and orientation of the arbitrary (x, y, z) system with respect to the (1, 2, 3) system, via the transformation

$$\begin{pmatrix} x \\ y \\ z \end{pmatrix} = \begin{pmatrix} \alpha_1 & \beta_1 & \gamma_1 \\ \alpha_2 & \beta_2 & \gamma_2 \\ \alpha_3 & \beta_3 & \gamma_3 \end{pmatrix} \begin{pmatrix} 1 \\ 2 \\ 3 \end{pmatrix} \quad \text{or } \boldsymbol{x} = \mathbf{T}\cdot\mathbf{1} \tag{17}$$

where $\mathbf{T}$ is the matrix of cosine directors. Thus, $\alpha_1 = \cos(x, 1)$, $\alpha_2 = \cos(y, 1)$, etc. It results from Equations 13–17 that to calculate the nine elastic moduli in the new coordinates system (x, y, z) one needs to know: (a) the nine direction cosines $\alpha_i, \beta_i, \gamma_i$, $(i = 1, 2, 3)$ and (b) the nine elastic constants (Young's and shear moduli, and Poisson's ratios) in the principal axes. Expressions for the nine elastic constants in the principal axes were discussed in the section on single lamellae. We now deal with the determination of direction cosines.

For the calculation of the direction cosines the following approach can be adopted. It is well known, since Euler, that the relative orientations of two coordinate systems may be specified by a set of three independent angles [50]. There is a large number of possible sequential choices for these three angles, and we adopt the following transformations from principal (or body) coordinates of the thin lamella to spatial (or arbitrary) coordinates of thick or "back-flip" lamellae, based on the specific requirements in our studies of bone micromechanics [9]. Starting with the principal axes typical of a thin lamella, and using the right-handed coordinate system described in Fig. 4, one first rotates the initial (principal) system of axes 123 by an angle ψ_1 clockwise about the 3 axis, and the new coordinate system is labelled $\xi\eta\zeta$. Next, the intermediate axes, $\xi\eta\zeta$, are rotated about the ξ axis counterclockwise by an angle ψ_2 to produce another intermediate set, the $\xi'\eta'\zeta'$ axes. Finally, the $\xi'\eta'\zeta'$ axes are rotated counterclockwise by an angle ψ_3 about the ζ' axis to produce the desired xyz system of axes. Fig. 4 illustrates the various stages of the sequence. The elements of the complete transformation $\mathbf{T}$ are obtained as the triple product of the

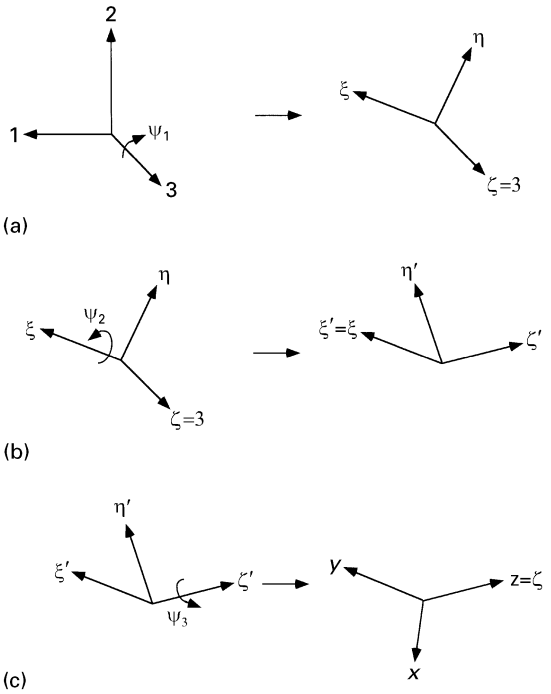

Figure 4 Rotations defining the Eulerian angles. (a) First rotation, ψ_1, clockwise about axis 3, (b) second rotation, ψ_2, counterclockwise about axis ξ; (c) third rotation, ψ_3, counterclockwise about axis ζ'.

individual rotations:

$$T_1 = \begin{pmatrix} \cos\psi_1 & -\sin\psi_1 & 0 \\ \sin\psi_1 & \cos\psi_1 & 0 \\ 0 & 0 & 1 \end{pmatrix}$$

$$T_2 = \begin{pmatrix} 1 & 0 & 0 \\ 0 & \cos\psi_2 & \sin\psi_2 \\ 0 & -\sin\psi_2 & \cos\psi_2 \end{pmatrix}$$

$$T_3 = \begin{pmatrix} \cos\psi_3 & \sin\psi_3 & 0 \\ -\sin\psi_3 & \cos\psi_3 & 0 \\ 0 & 0 & 1 \end{pmatrix} \qquad (18)$$

and thus, using Equation 17, one has $\boldsymbol{x} = \mathbf{T} \cdot \mathbf{1}$ where

$$\mathbf{T} = \mathbf{T}_3\mathbf{T}_2\mathbf{T}_1 = \begin{pmatrix} \cos\psi_1\cos\psi_3 + \sin\psi_1\cos\psi_2\sin\psi_3 & \cos\psi_1\cos\psi_2\sin\psi_3 - \sin\psi_1\cos\psi_3 & \sin\psi_2\sin\psi_3 \\ \sin\psi_1\cos\psi_2\cos\psi_3 - \cos\psi_1\sin\psi_3 & \cos\psi_1\cos\psi_2\cos\psi_3 + \sin\psi_1\sin\psi_3 & \sin\psi_2\cos\psi_3 \\ -\sin\psi_1\sin\psi_2 & -\cos\psi_1\sin\psi_2 & \cos\psi_2 \end{pmatrix} \qquad (19)$$

By identification of the elements of matrix $\mathbf{T}$ using Equations 17 and 19, the cosine directors α_i, β_i, and γ_i are now defined in terms of the elementary rotations, which are convenient from an experimental viewpoint.

As discussed, much of the variation within the structure of lamellar bone can be described in terms of the plywood angle ψ_1 which describes the extent of offset of the collagen fibril axes from the thin lamella to other lamella in a given lamellar unit and the rotation angle ψ_2 which describes the extent of rotation about the fibril axis relative to fibrils in the thin lamella. These two elementary rotations are modelled exactly by the first two rotations of the Eulerian transformation presented above. No third Eulerian angle ψ_3 is needed in this particular case in order to complete the transformation of the principal coordinates of the thin lamella into those of the thick or the "back-flip" lamella. Thus, $\psi_3 = 0^\circ$. Therefore, the matrix for the complete transformation from thin lamella to thick or "back-flip" lamellae is

$$T = \begin{pmatrix} \cos\psi_1 & -\sin\psi_1 & 0 \\ \sin\psi_1\cos\psi_2 & \cos\psi_1\cos\psi_2 & \sin\psi_2 \\ -\sin\psi_1\sin\psi_2 & -\cos\psi_1\sin\psi_2 & \cos\psi_2 \end{pmatrix} \qquad (20)$$

However, as the principal axes of the thin lamella are those which correspond (Fig. 3) to the major axes of bone, we are interested in the inverse transformation, namely, transforming the principal elastic constants of the thick and the "back-flip" lamellae into those in the principal axes of the thin lamella. Thus, the desired matrix of direction cosines should be that of the inverse transformation, which is actually the transposition of the matrix derived above, as we are dealing with an orthogonal transformation [50]. Thus, the matrix of direction cosines for the transformation of principal axes from thick or "back-flip" lamellae to thin lamella is

$$T^{-1} = \begin{pmatrix} \cos\psi_1 & \sin\psi_1\cos\psi_2 & -\sin\psi_1\sin\psi_2 \\ -\sin\psi_1 & \cos\psi_1\cos\psi_2 & -\cos\psi_1\sin\psi_2 \\ 0 & \sin\psi_2 & \cos\psi_2 \end{pmatrix} \qquad (21)$$

To conclude, a method is available for calculating the elastic moduli of the thick and "back-flip" lamellae in the principal axes of the thin lamella which correspond to the major axes of bone. For simplicity, the elastic moduli of the intermediate lamellae (i.e. the transition zone) in the major axes of bone are assumed here to be the mathematical average of the corresponding moduli of the thin and thick lamellae. More accurate calculations should take into account the exact contributions of the lamellae constituting the transition zone but this awaits the determination of the values of the rotational angle, ψ_2, for each of these lamellae which has not, as yet, been measured.

Assuming the thicknesses of the four types of lamellae to be T^{thick}, T^{thin}, T^{trans} and T^{bf} with a total lamellar unit thickness of $T = T^{\text{thick}} + T^{\text{thin}} + T^{\text{trans}} + T^{\text{bf}}$, the elastic moduli of bone in its major axes may be assumed to be given by

$$D_{kl}^{\text{Bone}} = \frac{1}{T}(T^{\text{thin}}D_{kl}^{\text{thin}} + T^{\text{thick}}D_{kl}^{\text{thick}} + T^{\text{trans}}D_{kl}^{\text{trans}} + T^{\text{bf}}D_{kl}^{\text{bf}}) \qquad (22)$$

where D_{kl}^{Bone} stands for the overall elastic moduli E, G and ν of bone in its principal axes $k, l (k, l =$ BA, TA, RA), and D_{kl}^{thin}, D_{kl}^{thick}, D_{kl}^{trans}, D_{kl}^{bf} stand for the elastic constants of the thin lamellae, thick lamellae, the transition zone and the "back-flip" lamellae, respectively, in the same major axes of bone.

2.3. Young's modulus of bone in an arbitrary direction

Knowing the principal elastic constants of parallel fibred bone (or lamellar bone), we are now also interested in calculating their Young's modulus in any direction in space. It is more convenient to do so by expressing E along an arbitrary direction in space in terms of spherical coordinates. One possibility is to rotate the rigid framework of principal axes of parallel fibred bone (or the rigid framework of principal axes of lamellar bone) such that the "1" axis (or the bone axis) would point into that arbitrary direction. This is performed (Fig. 5) by first rotating the framework by an angle, φ, clockwise about the "1" axis (or the bone axis) and then by an angle, θ, clockwise about the new "3" axis (or the new radial axis). The matrix of transformation is, thus

$$\begin{pmatrix} \cos\theta & -\sin\theta & 0 \\ \sin\theta & \cos\theta & 0 \\ 0 & 0 & 1 \end{pmatrix} \begin{pmatrix} 1 & 0 & 0 \\ 0 & \cos\varphi & -\sin\varphi \\ 0 & \sin\varphi & \cos\varphi \end{pmatrix}$$

$$= \begin{pmatrix} \cos\theta & -\sin\theta\cos\varphi & \sin\theta\sin 6 \\ \sin\theta & \cos\theta\cos\varphi & -\cos\theta\sin\varphi \\ 0 & \sin\varphi & \cos\varphi \end{pmatrix} \quad (23)$$

Thus, the direction cosines $\alpha_1, \beta_1, \gamma_1$ needed for the calculation of the Young's modulus of parallel fibred bone in an arbitrary direction in space defined by the spherical coordinates θ, φ (Fig. 5), using Equation 13, are now $\alpha_1 = \cos\theta$, $\beta_1 = -\sin\theta\cos\varphi$, $\gamma_1 = \sin\theta\sin\varphi$. Substituting $\alpha_1, \beta_1, \gamma_1$ into Equation 13 one gets

$$E(\theta,\varphi) = \left(\frac{\cos^4\theta}{E_1} + \frac{\sin^4\theta\cos^4\varphi}{E_2} + \frac{\sin^4\theta\sin^4\varphi}{E_3} + \cos^2\theta\sin^2\theta\cos^2\varphi I_{12} + \sin^4\theta\sin^2\varphi\cos^2\varphi I_{23} + \sin^2\theta\cos^2\theta\sin^2\varphi I_{31} \right)^{-1} \quad (24)$$

where

$$I_{ij} = \frac{1}{G_{ij}} - 2\frac{\nu_{ij}}{E_{ii}} \quad (i, j = 1, 2, 3 \; i \neq j) \quad (25)$$

Thus, Young's modulus of parallel fibred bone in the space defined by the 1–2, 2–3, and 3–1 planes ($0^\circ \leqslant \theta \leqslant 90^\circ$, $0^\circ \leqslant \varphi \leqslant 90^\circ$) is given as a function of its elastic constants in its principal directions and the spherical coordinates, θ, φ, as defined above. Equation 24 is valid for the calculation of the three-dimensional Young's modulus of lamellar bone in the space defined by the BA–TA. TA–RA, and RA–BA, as well, with the bone axis (BA), tangential axis (TA), and radial axis (RA) replacing "1", "2", and "3" axes of parallel fibred bone, respectively (Fig. 5).

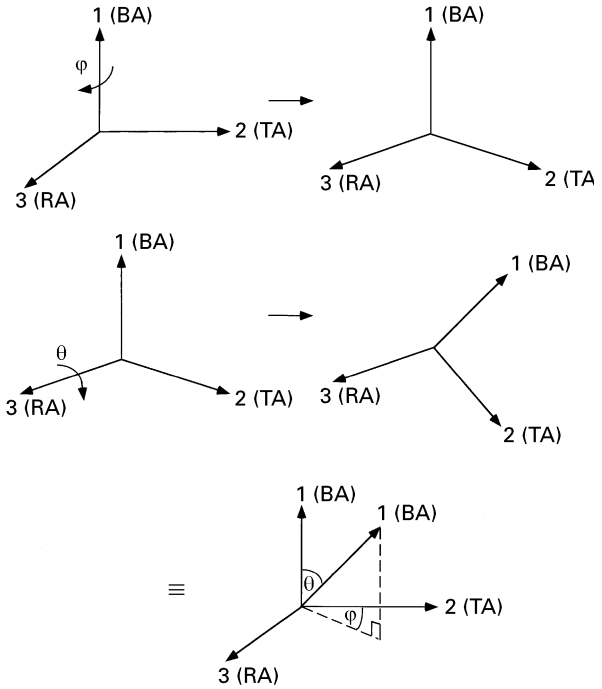

Figure 5 Definition of direction in space for parallel-fibred bone (or for lamellar bone) by spherical coordinates. (a) First rotation, φ, clockwise about the "1" axis (or the bone axis); (b) second rotation, θ, clockwise about the "3" axis (or the radial axis). The subsequent rotations result in the "1" axis (or the bone axis) pointing to the specific direction in space defined by θ and φ with regard to its orientation in the original system of coordinates. Letting $0^\circ \leqslant \theta \leqslant 90^\circ$ and $0^\circ \leqslant \varphi \leqslant 90^\circ$ the whole three-dimensional space defined by the 1–2, 2–3, and 3–1 planes of parallel-fibred bone (or the BA–TA, TA–RA, and RA–BA planes of lamellar bone) is covered.

3. Strategy

The elastic constants of platelet-reinforced parallel-fibred bone in its principal axes are first calculated using the HT, PB and LWX models with the parameters listed in Table II. Next Young's modulus of platelet-reinforced parallel-fibred bone in three-dimensional space is calculated using Equation 24. For this purpose, only the HT model is used as it contains expressions for all nine elastic constants which are necessary for three-dimensional calculations. For comparison, Young's moduli of platelet-reinforced parallel-fibred bone in the 1–2 plane are calculated for the HT, PB and LWX models, and the results for the cases of platelet, ribbon and sheet reinforcement are compared.

The calculated elastic constants in the principal axes of a single UPP platelet-reinforced lamella are used to calculate (using Equations 13–16) the stiffness constants of individual thin, thick, and "back-flip" lamellae in the major axes of bone. The orientations of the latter two lamellae relative to the thin lamella in terms of ψ_1 and ψ_2 are (Table I) $\psi_1 = 90^\circ$ and $\psi_2 = 70^\circ$, $\psi_1 = 120^\circ$ and $\psi_2 = 90^\circ$, respectively. The values of the stiffness constants of the transition zone in the major axes of bone are taken as the average

value of the respective thick and thin moduli. Using the relative lamellae thicknesses listed in Table I, the overall elastic constants of lamellar bone in its major axes are calculated using Equation 22. The three-dimensional Young's modulus of lamellar bone is calculated by introducing the latter results into Equation 24. The model for rotated plywood lamellar bone structure is then examined with respect to several variables and is compared to existing experimental data.

4. Results

4.1. Parallel-fibred bone

Fig. 6 shows the three-dimensional Young's modulus of parallel-fibred bone using the HT model for platelet reinforcement. A highly anisotropic structure is revealed with values of $E_1 = 33.6$ GPa, $E_2 = 24.3$ GPa and $E_3 = 3.0$ GPa for the Young's moduli in the principal axes of parallel-fibred bone. Young's modulus of parallel-fibred bone in the 1–2 plane ($\varphi = 0$), as calculated using the three different models is reported in Fig. 7. The HT, PB and LWX models all yield similar trends for the relation between stiffness and angle θ. These similarities are expected because the assumption of orthotropy is made in all models. The differences in three curves are due only to the different expressions for E_1 and E_2 used in Equation 24 One striking feature is the presence of a local maximum at a value of $\theta \neq 0^\circ$ or 90° for $\varphi = 0^\circ$ (1–2 plane). This maximum progressively disappears (Fig. 6) as φ increases. As discussed by Wagner and Weiner [7], it can be shown [51, 52] that for $\varphi = 0^\circ$, $E(\theta, \varphi)$ has a maximum different from both E_1 and E_2 for some values of θ other than 0° and 90° if

$$G_{12} > \frac{E_1}{2(1 + \nu_{12})} \tag{26}$$

and, similarly, $E(\theta, \varphi)$ has a minimum different from both E_1 and E_2 for some values of θ other than 0° and 90° if

$$G_{12} < \frac{E_1}{2[(E_1/E_2) + \nu_{12}]} \tag{27}$$

The extremum (minimum or maximum) occurs at the values of θ which satisfy

$$\tan^2 \theta = \frac{(2/E_1) + (2\nu_{12}/E_1) - (1/G_{12})}{(2/E_2) + (2\nu_{12}/E_1) - (1/G_{12})} \tag{28}$$

Thus, for example, using the HT model, the following elastic constants are calculated for parallel-fibred bone in the 12 plane ($\varphi = 0^\circ$): $E_1 = 33.6$ GPa, $E_2 = 24.3$ GPa, $G_{12} = 19.8$ GPa and $\nu_{12} = 0.34$. Substituting these values into Equations 26 and 27 a value of 12.5 GPa for the right-hand side of Equation 26 and a value of 9.8 GPa for the right-hand side of Equation 27 are obtained. This fulfils the conditions of Equation 26 but not of Equation 27, implying that E will have a maximum between 0° and 90°. For Equation 28, this maximum is calculated to occur at $\theta \approx 37^\circ$.

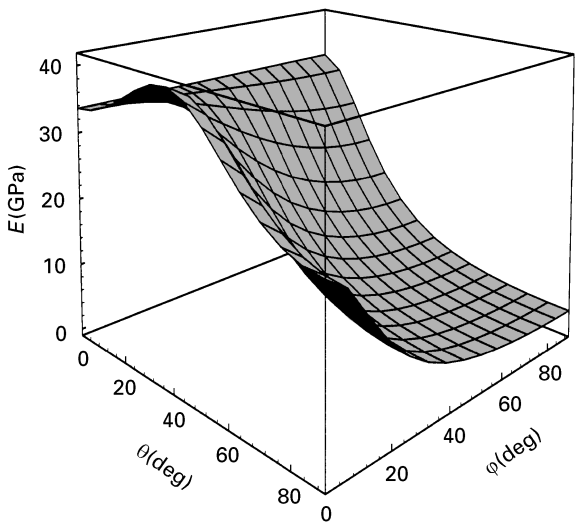

Figure 6 Three-dimensional Young's moduli of parallel-fibred bone (HT model) in the space defined by the 1–2 plane ($\varphi = 0^\circ$), 1–3 plane ($\varphi = 90^\circ$), nd 2–3 plane ($\theta = 90^\circ$).

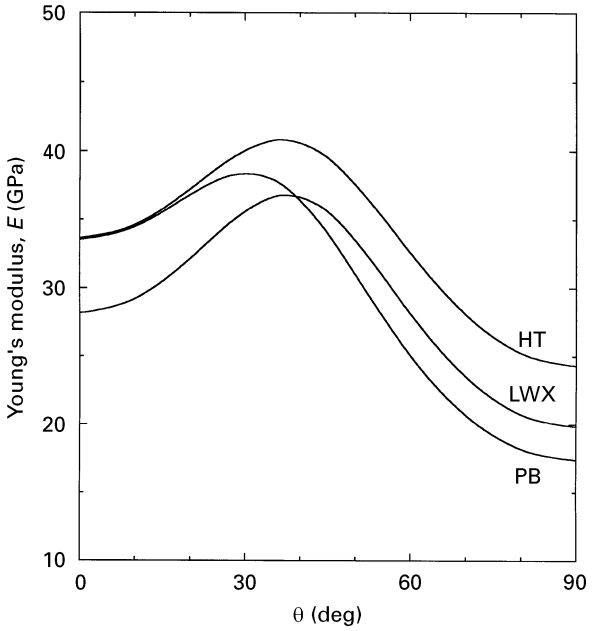

Figure 7 Young's modulus of parallel-fibred bone in the 1–2 plane ($\varphi = 0^\circ$) as calculated by the three different models (HT, PB, LWX).

The cases of ribbon and sheet reinforcement as compared to platelet reinforcement in parallel-fibred bone are shown in Fig. 8. Ribbon reinforcement enhances the Young's modulus of parallel-fibred bone in the longitudinal direction of the reinforcement from 33.6 GPa (platelet reinforcement) to 57.5 GPa. The Young's modulus in the other two directions remain the same as for platelets. For the case of sheet reinforcement $E_1 = E_2 = 57.5$ GPa, whereas E_3 does not change. Note, that in the mid-range of the θ angle (around $30^\circ < \theta < 60^\circ$) Young's modulus shows an intermediate value for ribbon reinforcement, whereas for sheets, as for platelets, there is a local maximum of the Young's modulus in this range.

4.2. Lamellar bone

The three-dimensional Young's modulus of lamellar bone as calculated using the HT model for the structural

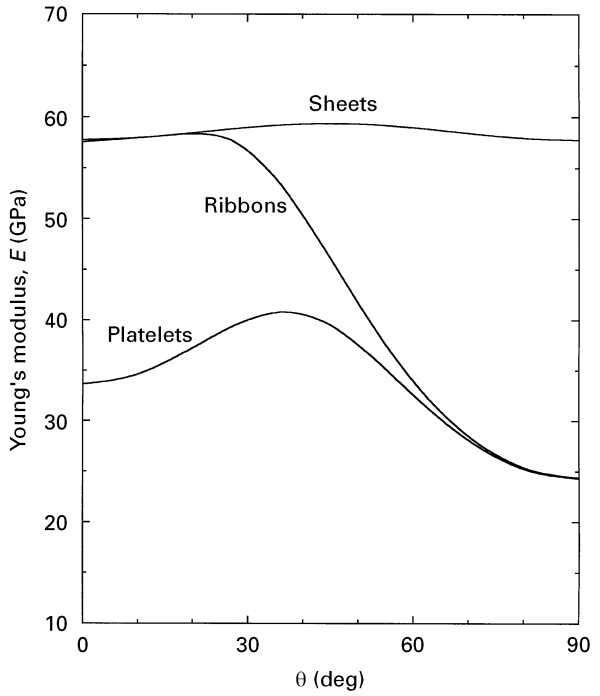

Figure 8 Young's modulus in the 1–2 plane ($\varphi = 0°$) of platelet, ribbon- and sheet-reinforced parallel-fibred bone (HT model).

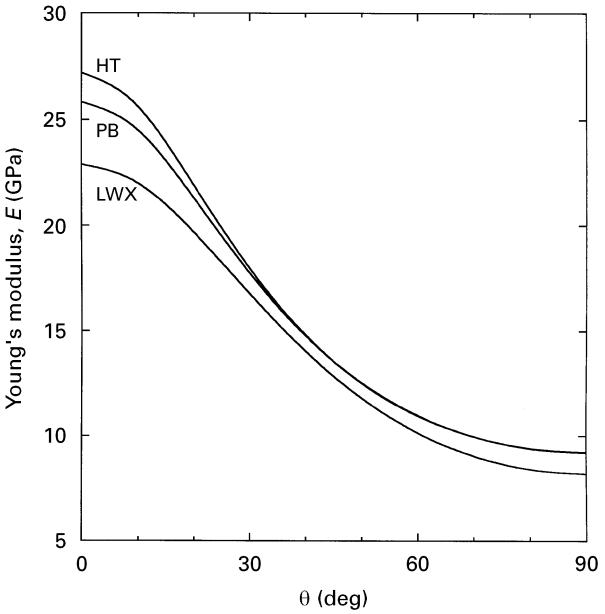

Figure 10 Young's modulus of lamellar bone in the bone axis–tangential axis plane ($\varphi = 0°$) as calculated by the three different models (HT, PB, LWX) for the material and structural parameters listed in Table I.

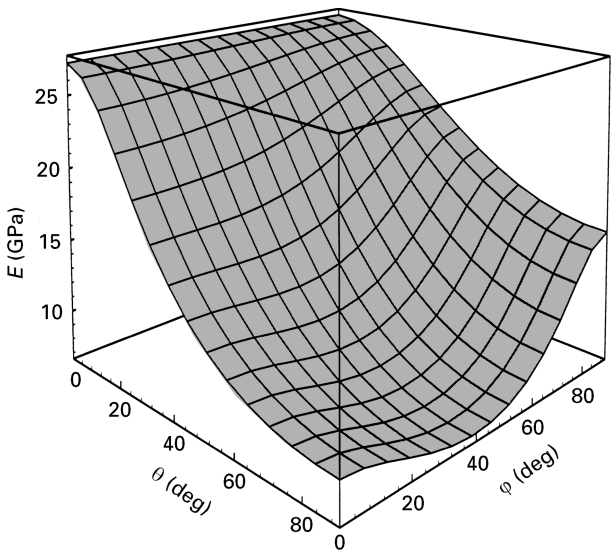

Figure 9 Three-dimensional Young's moduli of lamellar bone as calculated for the material and structural parameters listed in Table I in the space defined by the bone axis–tangential axis plane ($\varphi = 0°$), bone axis–radial axis plane ($\varphi = 90°$), and tangential axis–radial axis plane ($\theta = 90°$).

parameters listed in Table I versus the load direction in space, as defined by the spherical coordinates θ, φ, is shown in Fig. 9. The structure is clearly anisotropic. The calculated Young's modulus values in the three orthogonal directions are shown in Table III. Young's modulus of bone in the bone axis–tangential axis plane, as determined using the Halpin–Tsai, Padawer and Beecher and the Lusis *et al.* models, is shown in Fig. 10. All three models show a smoothly decreasing trend in Young's modulus from the bone axis value to the tangential axis. Note that the HT and LWX models give approximately the same values (26–27 GPa and ~9 GPa) for the Young's modulus in the bone axis and tangential axis, respectively, whereas the LWX model gives lower results (~23 GPa and ~8 GPa).

Table III also lists values for the Young's modulus in the bone axis and tangential axis (both calculated by the LWX model), and in the radial axis (calculated by the HT model) for various values of the rotational angle, Ψ_2, of the thick and "back-flip" lamellae. For each case, results for platelet, ribbon and sheet reinforcement are compared. Results for the specific case in which the "back-flip" lamella in a lamellar unit is absent, are also listed. Values of all other parameters (Table I) were kept constant. Note that Ψ_2 values of the rotated plywood structure are not known, and hence it is of interest to examine the sensitivity of the model to variations of Ψ_2. The case in which individual platelets adhere along their width dimension to form long bands, the longitudinal direction of which is the former width dimension of platelets ("transversally formed ribbons"), which is also structurally possible, is examined as well. Here, $W \to \infty$ (instead of L in Equations 4 and 7) and, thus, the rule of mixtures is obtained by all three models for E_2 but not for E_1 in an individual lamella. In addition, $A_{G_{12}} = (L/T)^{1.73}$ (Table II). All the other values of A for the remaining elastic moduli for ribbons (Table II) do not change. Table III shows that variations in Ψ_2 affect the Young's modulus values in the radial axis direction in particular. Furthermore, if the "back-flip" lamella is removed, the modulus values are much less isotropic. Table III also shows that the moduli for sheets and longitudinally formed ribbons as compared to platelets are extremely high in the bone axis (BA) direction, whereas for transversally formed ribbons, values of the Young's modulus in the bone axis are much closer to those of platelets.

TABLE III Data for Young's modulus of lamellar bone in the bone axis, tangential axis and radial axis directions for various values of the rotational angle, Ψ_2, and for the case in which the "back-flip" lamella is absent: (a) using parameters defined in Table I; (b) as in (a), but $\Psi_2 = 50^\circ$ for the thick lamella; (c) as in (a), but $\Psi_2 = 30^\circ$ for the "back-flip" lamella; (d) as in (a), but assuming no "back-flip" lamella present

	(a)				(b)			(c)			(d)	
Lamella "Back-flip" lamella	$\Psi_1 = 90^\circ$, $\Psi_2 = 70^\circ$ $\Psi_1 = 120^\circ$, $\Psi_2 = 90^\circ$				$\Psi_1 = 90^\circ$, $\Psi_2 = 50^\circ$ $\Psi_1 = 120^\circ$, $\Psi_2 = 90^\circ$			$\Psi_1 = 90^\circ$, $\Psi_2 = 70^\circ$ $\Psi_1 = 120^\circ$, $\Psi_2 = 30^\circ$			$\Psi_1 = 90^\circ$, Ψ_2 No "back-flip"	
	P	R	R*	S	P	R	S	P	R	S	P	R
E_1 (GPa)	22.9	41.2	24.6	48.4	22.9	41.2	48.4	25.3	44.1	51.3	26.2	48.8
E_2 (GPa)	8.3	13.6	6.5	13.6	9.5	14.6	14.8	10.0	15.1	15.4	9.2	15.9
E_3 (GPa)	13.6	12.8	24.4	24.5	9.2	8.6	16.1	10.7	9.8	14.4	12.2	11.1

P = platelet reinforcement; R = ribbon reinforcement; S = sheet reinforcement; R* = transversally formed ribbons (see text).

5. Discussion

The models presented here are based on our current understanding of the parallel-fibred and rotated plywood structures and their materials properties. The calculated values reflect the accuracies and inaccuracies both in our understanding of the *in vivo* structures and in the construction of the mathematical model, and of course do not take into account the considerably natural variation that exists in all bones. With so many unknowns, a fairly stringent way to test the model is to compare it to measured values of Young's modulus in different directions *via-a-vis* the bone axial directions, following the approach of Bonfield and Grynpas [24] and Reilly and Burstein [23]. Unfortunately, here too difficulties are encountered. No measured modulus values of pure parallel-fibred bone exist. All the measurements made are of fibrolamellar (also known as plexiform bone), which is a mixture of both parallel-fibred and lamellar bone. In the case of lamellar bone, our model is only relevant to a planar array of lamellae, and not to the far more complicated situation of osteonal bone, which is for the most part, a series of cylinders made up of folded lamellae [14]. No measurements of the Young's modulus of planar lamellar bone have been made to date, because of the relatively large specimen size needed. More or less planar arrays of circumferential lamellar bone are present in certain bones, but these are almost inevitably from small animals, and thus the volumes available for modulus measurements, are too small.

We have recently attempted partially to resolve this problem by making microhardness measurements on both pure parallel-fibred bone and planar lamellar arrays at different angles relative to the bone axes. The results are reported in Ziv *et al.* [15]. Although microhardness values cannot be directly related to Young's modulus, an approximate linear relation for bone has been observed[26, 53, 54, 55]. Ziv *et al.* [15] measured the microhardness values of parallel-fibred bovine bone in a zone close to the periosteum where lamellar bone is absent. Measurements were made along the three principal axes. It was found that each has a different value and that the differences are large (compared to lamellar bone), indicating a high degree of anisotropy. These trends are well reproduced in the model for platelets (cf. Figs 6 and 9 paying particular attention to the scales). Ziv *et al.* [15] also measured intermediate off-axis angles in order to determine whether or not the off-axis peak in Young's modulus predicted by Wagner and Weiner [7] is present. No such peak was found. Interestingly, the intermediate values measured are thus more consistent with the crystals being present in the form of ribbons rather than platelets (following Fig. 8) and it would be most interesting to try to evaluate this possibility by obtaining better *in vivo* information on crystal dimensions. Figs 11 and 12 compare two of the trends observed by Ziv *et al.* [15] for lamellar bone with the calculated (LWX model, platelet reinforcement, parameters as listed in Table I) modulus values for the same axial directions. The

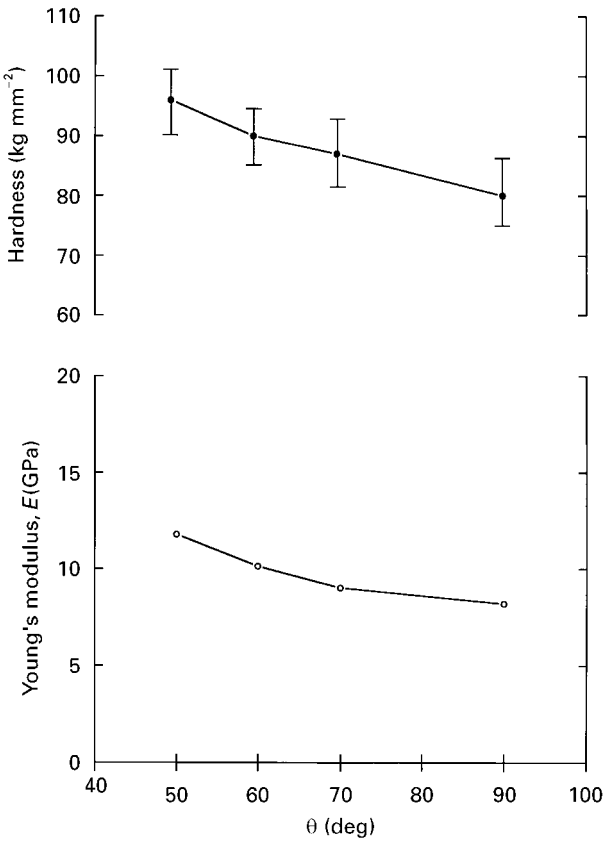

Figure 11 Trends in the microhardness measurements for the "a" set of planes [15] and in the Young's modulus of the corresponding directions in the bone axis–tangential axis plane, as calculated by the LWX model for platelet reinforced lamellar bone (material and structural parameters as listed in Table I).

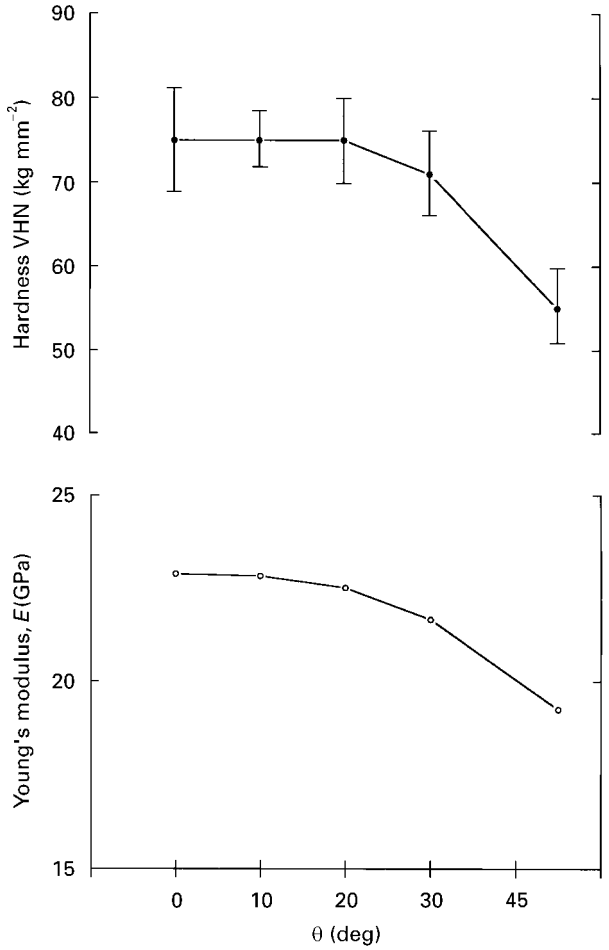

Figure 12 Trends in microhardness measurements for the "c" set of planes [15] and in the Young's modulus of the corresponding directions in the bone axis–radial axis plane, as calculated by the LWX model for platelet-reinforced lamellar bone (material and structural parameters as listed in Table I).

trends are remarkably similar, providing strong support for the validity of the model.

A comparison of the calculated values of Youngs' modulus with the measured modulus values for bulk fibrolamellar and osteonal bone are informative, despite the fact that they are not directly comparable. In general, the well-known measured anisotropy for fibrolamellar and osteonal bone [1] (higher values of Young's modulus in the bone axis direction relative to the radial and tangential directions) is consistently reproduced in our model for platelets, ribbons and sheets. Care must be taken when comparing the absolute values and trends measured with the calculated values for the reasons outlined above. We will restrict the discussion to osteonal bone measurements, as at least here we are dealing with only one structural type (as opposed to fibrolamellar bone). The relevant data sets of Reilly and Burstein [23] and Hasegawa *et al.* [56] range in Young's modulus values along the bone axis to the tangential or radial directions from 35 GPa to about 8 GPa. Our model using the structural parameters in Table I conforms well to this range for the cases of platelets and ribbons, but not sheets (Table III). The trends observed for off-axis measurements of Young's modulus of osteonal bone (Reilly and Burstein [23], Pidaparti *et al.* [25]) show a uniform decrease from the bone axis direction to the tangential/radial directions. Our model reproduces this trend well, but also predicts that the tangential and radial directions of planar lamellar sheets will have quite different absolute values (from Fig. 9). Such measurements, when available, could also provide indirect information on whether or not the dominant *in vivo* crystal shape of a given lamellar bone is in the form of platelets or ribbons, as these have (Table III) quite different tangential and radial values.

6. Conclusion

Relating bone structure, and, in particular, the lamellar structure common in mammalian bones, to mechanical properties, is indeed a very challenging task. The difficulties are not only due to the complex hierarchical structure and the necessity for measuring mechanical properties of very small specimens, but also to the considerable structural variation that is an inherent feature of biological materials. A flexible mechanical model is, therefore, an important means of overcoming some of these difficulties. A model of this type may also be useful for better understanding complex synthetic composite materials, and could, in particular, provide insights into the relative importance of the various structural features in terms of bulk material properties.

Acknowledgements

This study was funded by US Public Health Service grant (DE 06954) from the NIDR to S. W. S. W. holds the I.W. Abel Professorial Chair of Structural Biology.

References

1. J. D. CURREY, "The Mechanical Adapatations of Bones" (Princeton University Press, Princeton, NJ, 1984).
2. S. WEINER and W. TRAUB, *FASEB J.* **6** (1992) 879.
3. J. D. CURREY, *J. Bomech* **2** (1969) 1.
4. *Idem, ibid.* **2** (1969) 477.
5. S. WEINER, T. ARAD and W. TRAUB, *FEBS Lett.* **285** (1991) 49.
6. N. SASAKI, T. IKAWA and A. FUKUDA, *J. Biomech.* **24** (1991) 57.
7. H. D. WAGNER and S. WEINER, *ibid* **25** (1992) 1311.
8. J. D. CURREY, K. BREAR and P. ZIOUPOS, *ibid.* **27** (1994) 885.
9. W. J. LANDIS, M. J. SONG, A. LEITH, L. McEWEN and B. F. McEWEN, *J. Struct. Biol.* **110** (1993) 39.
10. R. STUHLER, *Forscht. Geb. Röntgenstrahlen* **57** (1937) 231.
11. R. A. ROBINSON, *J. Bone Surg.* **34A** (1952) 389.
12. E. WACHTEL and S. WEINER, *J. Bone. Miner. Res.* **9** (1994) 1651.
13. S. WEINER and P. A. PRICE, *Calcif. Tiss. Int.* **39** (1976) 365.
14. H. FRANCILLON-VIÉLLOT, V. DE BUFFERENÍL, J. CASTANET, J. GERAUDIE, F. J. MEUNIER, J. Y. SIRE, L. ZYLBERBERG and A. DE RICQLÉS, in "Skeletal Biomineralization Patterns, Processes and Evolutionary Trends", edited by J. G. Carter, Ch. 20, pp 471–530.
15. V. ZIV, H. D. WAGNER and S. WEINER, *Bone* **18** (1996) 417.
16. W. GEBHARDT, *Arch. Entw. Mech. Org.* **20** (1906) 187.
17. M. M. GIRAUD-GUILLE, *Calcif. Tiss. Int.* **42** (1988) 167.
18. S. A. REID, *Anat. Embryol.* **174** (1986) 329.
19. J. W. SMITH, *J. Bone Joint Surg.* **42B** (1960) 588.
20. G. MARROTI, *Calicif. Tiss. Int.* **53** (1993) 547.

21. S. WEINER, T. ARAD, I. SABANAY and W. TRAUB, *Bone*, in press.
22. V. ZIV, I. SABANAY, T. ARAD, W. TRAUB and S. WEINER, *Microsc. Res. Tech.* **33** (1996) 203.
23. D. T. REILLY and A. H. BURSTEIN, *J. Biomec-*. **8** (1975) 393.
24. W. BONFIELD and M. D. GRYNPAS, *Nature* **270** (1977) 453.
25. R. M. V. PIDAPARTI, A. CHANDRAN, Y. TAKANO and C. H. TURNER, *J. Biomech.* **29** (1996) 909.
26. G. P. EVANS, J. C. BEHIRI, J. D. CURREY and W. BONFIELD, *J. Mater. Sci. Mater. Med.* (1990) 38.
27. S. WEINER, T. ARAD and W. TRAUB, *Chem. Biol. Mineral. Tiss.* (1992) 93.
28. S. WEINER and W. TRAUB, *FEBS Lett*. **206** (1986) 262.
29. P. FRATZL, M. GROSCHNER, G. VOGEL, H. PLENK, Jr, J. ESCHBERGER, N. FRATZL-ZELMAN, K. KOLLER and K. KLAUSHOFER, *Bone Miner. Res.* **7** (1992) 329.
30. A. BOYDE, *Cell Tiss. Res.* **152** (1974) 543.
31. M. J. GLIMCHER, *Phil. Trans. R. Soc. Lond.* **B304** (1984) 479.
32. S. FITTON-JACKSON, *Proc. R. Soc. Lond. Ser. B.* **146** (1956) 270.
33. W. TRAUB, T. ARAD and S. WEINER, *Conn. Tiss. Res.* **28** (1992) 99.
34. A. L. ARSENAULT, *Calcif. Tiss. Res.* **6** (1991) 239.
35. E. P. KATZ, E. WACHTEL, M. YAMAUCHI and G. L. MECHANIC, *Conn. Tiss. Res.* **21** (1989) 149.
36. M. YAMAUCHI, E. P. KATZ, O. KAZUNORI, K. TERAOKA and G. L. MECHANIC, *ibid* **18** (1989) 41.
37. M. W. K. CHEW and J. M. SQUIRE, *Int. J. Biol. Macromol.* **8** (1986) 27.
38. H. J. HÖHLING, B. A. ASHTON and H. D. KOSTER, *Cell. Tiss. Res.* **148** (1974) 11.
39. S. DOTY, R. A. ROBINSON and B. SCHOFIELD, in "Handbook of Physiology," (edited by G. D. Aurbach, (American Physiology Society, Washington, DC, 1976) pp. 3–23.
40. R. S. GILMORE and J. L. KATZ, *J. Mater. Sci.* **17** (1982) 1131.
41. A. TANIOKA, T. TAZAWA, K. MIYASAKA and K. ISHIKAWA, *Biopolymers* **13** (1974) 735.
42. S. G. LEKHNITSKII, "Theory of Elasticity of an Anisotropic Elastic Body" (Holden-Day, San Francisco, 1963) pp. 1–73.
43. U. AKIVA, E. ITZHAK and H. D. WAGNER, *Compos. Sci. Tech.*, in press.
44. J. C. HALPIN, "Primer on Composite Materials: Analysis", Revised Edition (Technomic Publishing, Lancaster, PA, 1984) pp. 125–137.
45. G. E. PADAWER and N. BEECHER, *Polym. Engng Sci.* **10** (1970) 185.
46. J. LUSIS, R. T. WOODHAMS and M. XHANTOS, *ibid.* **13** (1973) 139.
47. L. E. NIELSEN, *J. Appl. Phys.* **41** (1970) 4626.
48. L. E. NIELSEN, "Mechanical Properties of Polymers and Composites", Vol. 2 (Marcel-Dekker, 1974) Ch. 8.
49. H. L. COX, *J. Appl. Phys.* **3** (1952) 72.
50. H. GOLDSTEIN, "Classical Mechanics" (Addison-Wesley, 1980) pp. 143–8 and Appendix B.
51. B. D. AGARWAL and L. J. BROUTMAN, "Analysis and Performance of Fiber Composites" (Wiley, New York, 1980).
52. B. GERSHON, D. COHN and G. MAROM, *Biomaterials* **11** (1990) 548.
53. J. D. CURREY and K. BREAR, *J. Mater. Sci. Mater. Med.* **1** (1990) 14.
54. G. P. EVANS, J. C. BEHIRI and W. BONFIELD, *Adv. Biomater*. **8** (1988) 311.
55. R. HODGSKINSON, J. D. CURREY and G. P. EVANS, *J. Orthop. Res.* **7** (1989) 754.
56. K. HASEGAWA, C. H. TURNER and D. B. BURR, *Calcif. Tiss. Int*. **55** (1994) 381.

Received 19 August
and accepted 20 August 1997